

Determination of the beam asymmetry Σ in η - and η' -photoproduction using Bayesian statistics

JAKOB MICHAEL KRAUSE

Masterarbeit in Physik
angefertigt im Helmholtz-Institut für Strahlen- und
Kernphysik

vorgelegt der
Mathematisch-Naturwissenschaftlichen Fakultät
der
Rheinischen Friedrich-Wilhelms-Universität
Bonn

Sep 2022

DRAFT

I hereby declare that this thesis was formulated by myself and that no sources or tools other than those cited were used.

Bonn,
Date

.....
Signature

- 1. Gutachterin: JUN. PROF. DR. ANNIKA THIEL
- 2. Gutachter: PROF. DR. JOCHEN DINGFELDER

DRAFT

Contents

1	Introduction	1
1.1	Photoproduction of Pseudoscalar Mesons	4
1.2	Measurement of Polarization Observables	5
1.3	Introduction to BAYESIAN statistics	5
1.4	Motivation and Structure of this Thesis	5
2	Experimental Setup	7
2.1	Production of (polarized) high energy photon beam	7
2.1.1	Tagger	8
2.2	Beam Target	8
2.3	Calorimeters	8
2.4	Trigger	8
3	Event selection	11
3.1	Preselection and charge cut	11
3.2	Time of particles	12
3.3	Kinematic constraints	14
3.3.1	Derivation of cut conditions	14
3.3.2	Determination of cut ranges	15
3.3.3	Quality of event selection	21
3.4	Investigation of background and additional cuts	22
3.4.1	Inspecting plausibility of background reactions	22
3.4.2	Misidentification of background reactions	25
3.4.3	Examination of additional cuts	28
3.5	Summary of event selection	31
4	Extraction of the beam asymmetries Σ_η and $\Sigma_{\eta'}$	33
4.1	Methods	34
4.1.1	Event yield asymmetries	34
4.1.2	Event based fit	37
4.2	Determination of Σ_η using Bayesian statistics	37
4.2.1	Event yield asymmetries	37
4.2.2	Event based fit	37
4.2.3	Discussion	37
4.3	Determination of $\Sigma_{\eta'}$	37
4.3.1	Application of event based fit to toy Monte Carlo data	37

4.3.2	Application of event based fit to data	37
4.3.3	Systematic Error	37
5	Summary and outlook	37
A.1	Statistical error for the asymmetry $A(\phi)$	5
	Bibliography	7
	List of Figures	9
	List of Tables	11

DRAFT

Extraction of the beam asymmetries Σ_η and $\Sigma_{\eta'}$

The beam asymmetry Σ is observable when a linearly polarized photon beam and unpolarized liquid hydrogen target are employed. The polarized cross section $\frac{d\sigma}{d\Omega_{\text{pol}}}$ is not symmetric in the azimuthal angle ϕ anymore as opposed to the unpolarized cross section $\frac{d\sigma}{d\Omega_0}$. It is rather modulated by a cosine dependence which scales with the polarization observable Σ and the (linear) beam polarization p_γ , see equation (4.1) [San+11].

$$\frac{d\sigma}{d\Omega_{\text{pol}}}(E_\gamma, \cos \theta, \phi) = \frac{d\sigma}{d\Omega_0}(E_\gamma, \cos \theta) \cdot \left[1 - p_\gamma \Sigma(E_\gamma, \cos \theta) \cos(2\phi) \right] \quad (4.1)$$

Since the incident photon beam is polarized, photon momentum \vec{k} and polarization $\vec{\epsilon}$ span a plane which is referred to as the beam polarization plane. This plane is tilted by the angle φ with respect to the reaction plane which is defined by the final state momenta. Naturally, this plane builds the angle ϕ in the laboratory system. At the same time the angle of the beam polarization plane in the same reference frame is defined as α . It holds

$$\varphi = \alpha - \phi. \quad (4.2)$$

Figure 4.1 illustrates definitions of all angles and planes. Theoretically the beam asymmetry can be

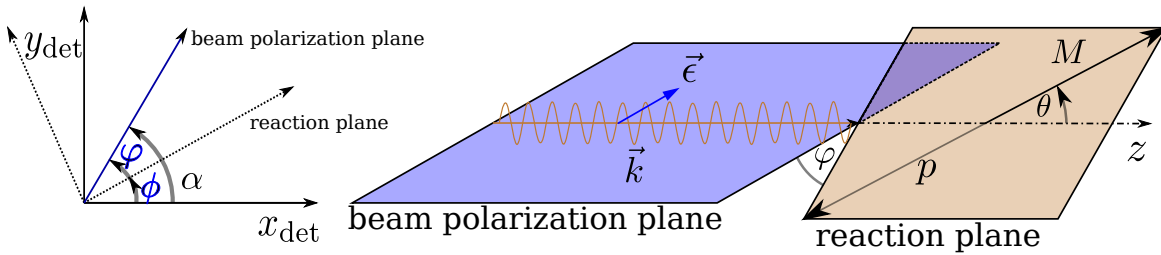


Figure 4.1: Left: Definition of angles α , ϕ , φ . Right: Photon momentum \vec{k} and polarization $\vec{\epsilon}$ define the beam polarization plane while the reaction plane is defined by the recoil proton p and produced meson M .

determined by a measurement of the cross section and a fit using equation (4.1). However, when calculating polarized cross sections, it is important to have good control over flux normalization and detector acceptance in three dimensions ($E_\gamma, \cos \theta, \phi$). To avoid this, the measurement of asymmetries

can be used to access the polarization observable Σ instead. Particularly, data is taken for two distinct orthogonal polarization settings corresponding to $\alpha = \pm 45^\circ$.

This chapter will illustrate the process of determining the beam asymmetry for η and η' photoproduction. The published results of Σ_η [Afz19; Afz+20] are used to check the accuracy and functionality of employed bayesian methods. Bayesian methods, as well as traditional frequentist approaches are used afterwards to extract new results for $\Sigma_{\eta'}$. First, the used methods will be presented and subsequently their application for each final state, respectively.

4.1 Methods

The beam asymmetry has to be determined via fits to ϕ distributions obtained from data. These are performed as either binned or unbinned fits. Both methods allow the application of Bayesian methods as will be discussed in the following. Additionally the advantages and disadvantages of all methods are compared.

4.1.1 Event yield asymmetries

Measurements were made in two distinct polarization settings $\alpha = \pm 45^\circ = \alpha^{\perp/\parallel}$. Thus, the polarized cross sections for both settings are given by¹

$$\frac{d\sigma^{\parallel}}{d\Omega_{\text{pol}}} = \frac{d\sigma}{d\Omega_0} \cdot \left[1 - p_\gamma^{\parallel} \Sigma \cos \left(2 \left(\alpha^{\parallel} - \phi \right) \right) \right] \quad (4.3)$$

and

$$\frac{d\sigma^{\perp}}{d\Omega_{\text{pol}}} = \frac{d\sigma}{d\Omega_0} \cdot \left[1 - p_\gamma^{\perp} \Sigma \cos \left(2 \left(\alpha^{\perp} - \phi \right) \right) \right] \quad (4.4)$$

$$= \frac{d\sigma}{d\Omega_0} \cdot \left[1 + p_\gamma^{\perp} \Sigma \cos \left(2 \left(\alpha^{\parallel} - \phi \right) \right) \right]. \quad (4.5)$$

Note that equation (4.5) holds, because

$$\alpha^{\perp} = \alpha^{\parallel} + \pi/2 \quad \text{and} \quad \cos x = -1 \cdot \cos(x + \pi).$$

Consider now taking the difference of equations (4.3) and (4.5)

$$\frac{d\sigma^{\perp}}{d\Omega_{\text{pol}}} - \frac{d\sigma^{\parallel}}{d\Omega_{\text{pol}}} = \frac{d\sigma}{d\Omega_0} \cdot \left(p_\gamma^{\perp} + p_\gamma^{\parallel} \right) \Sigma \cos \left(2 \left(\alpha^{\parallel} - \phi \right) \right). \quad (4.6)$$

One can further eliminate the unpolarized cross section from this equation by dividing by the polarization weighted sum of equations (4.3) and (4.5)

$$\alpha \cdot \frac{d\sigma^{\parallel}}{d\Omega_{\text{pol}}} + \beta \cdot \frac{d\sigma^{\perp}}{d\Omega_{\text{pol}}} = \frac{d\sigma}{d\Omega_0} \cdot \left[\alpha + \beta - \left(\alpha p_\gamma^{\parallel} - \beta p_\gamma^{\perp} \right) \Sigma \cos \left(2 \left(\alpha^{\perp} - \phi \right) \right) \right] \stackrel{!}{=} 2 \frac{d\sigma}{d\Omega_0}. \quad (4.7)$$

¹ The dependencies of polarized and unpolarized cross sections as well as the beam asymmetry like in equation (4.1) are implied

Since

$$\frac{d}{d\phi} \frac{d\sigma}{d\Omega_0} \stackrel{!}{=} 0 \forall \phi,$$

it holds

$$\alpha p_\gamma^\parallel - \beta p_\gamma^\perp \stackrel{!}{=} 0 \quad \alpha + \beta \stackrel{!}{=} 2, \quad (4.8)$$

such that

$$\alpha = \frac{2p_\gamma^\parallel}{p_\gamma^\perp + p_\gamma^\parallel} \quad \beta = \frac{2p_\gamma^\perp}{p_\gamma^\perp + p_\gamma^\parallel}. \quad (4.9)$$

The beam asymmetry Σ is thus accessible via the asymmetry

$$A(\phi) = \frac{\frac{d\sigma^\perp}{d\Omega_{\text{pol}}} - \frac{d\sigma^\parallel}{d\Omega_{\text{pol}}}}{p_\gamma^\parallel \frac{d\sigma^\perp}{d\Omega_{\text{pol}}} + p_\gamma^\perp \frac{d\sigma^\parallel}{d\Omega_{\text{pol}}}} = \Sigma \cos \left(2 \left(\alpha^\parallel - \phi \right) \right). \quad (4.10)$$

At this point one can now make use of the fact that in any scattering reaction the number of events N is given by the product of luminosity L and total cross section σ

$$N = L \cdot \sigma = \Phi \cdot N_t \cdot \frac{d\sigma}{d\Omega} \cdot \Delta\Omega,$$

where Φ is the beam flux, N_t the number of target particles and $\Delta\Omega$ is the solid angle covered by the detector. Substituting this in equation (4.10) one can build the asymmetry $A(\phi)$ using only the (flux-)normalized event yields $\tilde{N}^{\parallel/\perp} \left(E_\gamma, \cos \theta, \phi \right)^2$

$$A(\phi) = \frac{\tilde{N}^\perp - \tilde{N}^\parallel}{p_\gamma^\parallel \tilde{N}^\perp + p_\gamma^\perp \tilde{N}^\parallel} = \Sigma \cos \left(2 \left(\alpha^\parallel - \phi \right) \right). \quad (4.11)$$

Alternatively, the event yields N can also be normalized by integrating over the total azimuthal angle range in each bin of $(E_\gamma, \cos \theta)$. This normalization technique has been used in reference [Afz19] and will also be used in this work. Using appropriate binning in ϕ in addition to beam energy and meson polar angle the asymmetry can be build for all kinematic bins and the beam asymmetry then be extracted via a one-Parameter fit. The statistical errors for $A(\phi)$ are given by GAUSSIAN error propagation (see appendix A.1).

Frequentist

The beam asymmetry can now be determined via a frequentist fit, where Σ is determined such that the χ^2 value resulting from the data points and equation 4.11 is minimized. The results are point estimates with statistical error bars that are also obtained from the fit: $\hat{\Sigma} \pm \sigma_{\hat{\Sigma}}$. In addition $\chi^2/\text{NDF} \approx 1$ may be verified in order to diagnose the fit itself. Multiple automated minimization and calculation

² again, arguments $(E_\gamma, \cos \theta, \phi)$ are implied.

algorithms for χ^2 fitting are available as open source. The *Python* [RP22] module *scipy* [Vir+20] and *ROOT* [BR97] offer e.g. the methods `scipy.optimize.curve_fit` [sci] and `TH1::Fit()` [ROO] for discrete/binning data, which were used in the analysis.

Bayesian

Following section ??, where the basics of BAYESIAN inference were discussed, the goal of a BAYESIAN approach is to sample marginal posterior distributions for each fitted parameter from the joint posterior $p(\boldsymbol{\theta}|y)$ which depends on the observed data y . The joint posterior itself is proportional to the product of priors $\pi(\boldsymbol{\theta})$ and likelihood $\mathcal{L}(y|\boldsymbol{\theta})$ (BAYES' theorem)

$$p(\boldsymbol{\theta}|y) \propto \pi(\boldsymbol{\theta}) \cdot \mathcal{L}(y|\boldsymbol{\theta}). \quad (4.12)$$

This collapses to a one parameter problem in the case of fitting the event yield asymmetries (Eq. (4.11))

$$p(\Sigma|y) \propto \pi(\Sigma) \cdot \mathcal{L}(y|\Sigma). \quad (4.13)$$

However, to be able to sample from a joint posterior, prior and likelihood need to be specified. In order not to bias the fit towards any particular values, the prior is chosen non-informative, realized by a broad GAUSSIAN centered at 0 which is truncated to the physically allowed parameter space of $\Sigma \in [-1, 1]$. Furthermore, the likelihood is formulated assuming GAUSSIAN errors ϵ_n at each data point y_n , which should be described by the asymmetry (Eq (4.11)) at bin n $A(\phi_n; \Sigma)$, i. e.

$$\Sigma \sim \text{normal}(0, 1) \quad y_n = A(\phi_n; \Sigma) + \epsilon_n \quad \epsilon_n \sim \text{normal}(0, \sigma_n), \quad (4.14)$$

which is equivalent to

$$\Sigma \sim \text{normal}(0, 1) \quad y_n \sim \text{normal}(A(\phi_n; \Sigma), \sigma_n). \quad (4.15)$$

The likelihood of all data points now evaluates to

$$\mathcal{L}(y|\Sigma) = \prod_n y_n, \quad (4.16)$$

such that all ingredients are present to form a fully BAYESIAN probabilistic model. This model was implemented in Stan [Sta22], directly giving access to samples from the posterior obtained with the No-U-Turn-Sampler (NUTS) [Sta22; HG14]. Hereby, the sampling is restricted to the allowed parameter region $\Sigma \in [-1, 1]$. As a measure of goodness of fit, the p -values obtained from the posterior predictive distributions, as introduced in section ??, are reviewed. To diagnose the convergence of the MCMC fit, sensible values for \hat{R} and the Monte-Carlo standard error σ_{MCSE} are verified.

4.1.2 Event based fit

Frequentist

Bayesian

4.2 Determination of Σ_η using Bayesian statistics

4.2.1 Event yield asymmetries

Application of method to toy Monte Carlo data

Application of method to data

4.2.2 Event based fit

Application of method to toy Monte Carlo data

Application of method to data

4.2.3 Discussion

4.3 Determination of $\Sigma_{\eta'}$

4.3.1 Application of event based fit to toy Monte Carlo data

4.3.2 Application of event based fit to data

4.3.3 Systematic Error

Bibliography

- [San+11] A. M. Sandorfi, S. Hoblit, H. Kamano and T.-S. H. Lee,
Determining pseudoscalar meson photoproduction amplitudes from complete experiments,
Journal of Physics G: Nuclear and Particle Physics **38** (2011) 053001, ISSN: 1361-6471,
URL: <http://dx.doi.org/10.1088/0954-3899/38/5/053001> (cit. on p. 33).
- [Afz19] F. N. Afzal, *Measurement of the beam and helicity asymmetries in the reactions*
 $\gamma p \rightarrow p\pi^0$ and $\gamma p \rightarrow p\eta$,
PhD thesis: Rheinische Friedrich-Wilhelms-Universität Bonn, 2019,
URL: <https://hdl.handle.net/20.500.11811/8064> (cit. on pp. 34, 35).
- [Afz+20] F. Afzal et al.,
Observation of the $p\eta$ Cusp in the New Precise Beam Asymmetry Σ Data for $\gamma p \rightarrow p\eta$,
Phys. Rev. Lett. **125** (15 2020) 152002,
URL: <https://link.aps.org/doi/10.1103/PhysRevLett.125.152002>
(cit. on p. 34).
- [RP22] G. van Rossum and the Python development team,
The Python Language Reference, Release 3.10.5, 2022,
URL: <https://docs.python.org/3.10/reference/index.html> (cit. on p. 36).
- [Vir+20] P. Virtanen et al., *SciPy 1.0: Fundamental Algorithms for Scientific Computing in Python*,
Nature Methods **17** (2020) 261 (cit. on p. 36).
- [BR97] R. Brun and F. Rademakers, *ROOT — An object oriented data analysis framework*,
Nucl. Instrum. Meth. A **389** (1997) 81, ISSN: 0168-9002, URL:
<https://www.sciencedirect.com/science/article/pii/S016890029700048X>
(cit. on p. 36).
- [sci] scipy, *scipy.optimize.curve_fit, Function Documentation*,
URL: https://docs.scipy.org/doc/scipy/reference/generated/scipy.optimize.curve_fit.html (visited on 28/06/2022) (cit. on p. 36).
- [ROO] ROOT, *TH1 Class reference*, URL: <https://root.cern.ch/doc/master/classTH1.html#a63eb028df86bc86c8e20c989eb23fb2a> (visited on 28/06/2022) (cit. on p. 36).
- [Sta22] Stan development team, *Stan Modeling Language Users Guide and Reference Manual*,
vol. 2.29, 2022, URL: <https://mc-stan.org> (cit. on p. 36).
- [HG14] M. D. Hoffman and A. Gelman,
The No-U-Turn Sampler: Adaptively Setting Path Lengths in Hamiltonian Monte Carlo,
Journal of Machine Learning Research **15** (2014) 1593,
URL: <http://jmlr.org/papers/v15/hoffman14a.html> (cit. on p. 36).

List of Figures

1.1	Running coupling of QCD. The colored data points represent different methods to obtain a value for α_s . For more details it may be referred to [pdg]	2
1.2	Calculated nucleon (isospin $I = 1/2$) resonances compared to measurements. Left in each column are the calculations [bonnmodel] , the middle shows the measurements and PDG rating [pdg]	3
1.3	FEYNMAN diagram for the s-channel photoproduction of pseudoscalar mesons, adapted from [Afz19]	4
2.1	[cb]	7
2.2	[cb]	8
2.3	[cb]	8
2.4	D. WALTHER in [urban]	9
2.5	[cb]	9
2.6	[cb]	10
3.1	Distribution of event classes in $\eta' \rightarrow \gamma\gamma$ production	12
3.2	Time information of all final state particles and the beam photon for 3PED η' production	13
3.3	Reaction time t_r for 3PED η' production	14
3.4	Coplanarity of the $p\eta'$ final state with all other cuts applied for the energy bin $1\,500\,\text{MeV} \leq E_\gamma < 1\,600\,\text{MeV}$. The vertical dashed lines show the cut ranges obtained from a gaussian fit to the data (open circles). The solid black histograms represent fitted MC data of $\eta' \rightarrow \gamma\gamma$	18
3.5	Polar angle difference of the $p\eta'$ final state with all other cuts applied for the energy bin $1\,500\,\text{MeV} \leq E_\gamma < 1\,600\,\text{MeV}$. The vertical dashed lines show the cut ranges obtained from a gaussian fit to the data (open circles). The solid black histograms represent fitted MC data of $\eta' \rightarrow \gamma\gamma$	18
3.6	Missing mass of the $p\eta'$ final state with all other cuts applied for the energy bin $1\,500\,\text{MeV} \leq E_\gamma < 1\,600\,\text{MeV}$. The vertical dashed lines show the cut ranges obtained from a fit to data (open circles) employing a Novosibirsk function. The solid colored histograms represent fitted MC data from relevant photoproduction reactions: in black η' , in green π^0 , in red η , in blue ω , in yellow $2\pi^0$, magenta $\pi^0\eta$. The turquoise histogram is the sum of all MC histograms.	19

3.7	Invariant mass of the $p\eta'$ final state with all other cuts applied for all energy and angular bins. The open circles represent the measured data, the solid colored histograms fitted MC data from relevant photoproduction reactions: in black η' , in green π^0 , in red η , in blue ω , in yellow $2\pi^0$ and in magenta $\pi^0\eta$. The turquoise histogram is the sum of all MC histograms.	20
3.8	Invariant mass of the $p\eta'$ final state with all other cuts applied for the energy bin $1\,500\text{ MeV} \leq E_\gamma < 1\,600\text{ MeV}$. The vertical dashed lines show the cut ranges obtained from a gaussian fit to the η' MC data (solid black histogram). The open circles represent the measured data, the solid colored histograms fitted MC data from relevant photoproduction reactions: in black η' , in green π^0 , in red η , in blue ω , in yellow $2\pi^0$ and in magenta $\pi^0\eta$. The turquoise histogram is the sum of all MC histograms.	21
3.9	Acceptance for the reaction $\gamma p \rightarrow p\eta'$ after all cuts that have been discussed so far for 2.5PED and 3PED events	22
3.10	Fraction of background events in the analyzed beam energy and angular bins.	23
3.11	Acceptance for possible background contributions	24
3.12	Generated energies of the two lowest energy photons in $2\pi^0$ photoproduction MC data. The threshold of 20 MeV is marked by a vertical red line. Lowest energy photon is shown on the top, second lowest energy photon is shown on the bottom.	25
3.13	Generated energies of the two lowest energy photons in $2\pi^0$ and $\pi^0\eta$ photoproduction MC data. The threshold of 20 MeV is marked by a vertical red line. Lowest energy photon is shown on the top, second lowest energy photon is shown on the bottom.	26
3.14	Polar angle difference $\Delta\theta$ between the photon with second highest energy and second lowest energy of the $\pi^0\eta$ final state.	26
3.15	Illustration of the misidentification process during reconstruction	27
3.16	Generated CMS angle $\cos\theta_{\text{gen.}}$ vs. reconstructed CMS angle $\cos\theta_{\text{rec.}}$ for both background reactions. The slope $\cos\theta_{\text{gen.}} = \cos\theta_{\text{rec.}}$ is indicated by the solid line.	28
3.17	Detector hits of the recoil proton, as obtained from MC data for the production of η' , $2\pi^0$ and $\pi^0\eta$. CB: Crystal Barrel, FW: forward dector, MT: MiniTAPS	30
3.18	Difference in measured and calculated beam energy. Data points are shown as open circles, MC data as solid histograms: in black η' , in green π^0 , in red η , in blue ω , in yellow $2\pi^0$ and in magenta $\pi^0\eta$. The turquoise histogram is the sum of all MC histograms.	31
3.19	Invariant mass spectrum passing different stages in the event selection process. In the end clear peaks for all possibly produced mesons are visible. The vertical lines indicate the mean cut ranges over all energy and angle bins.	32
4.1	Left: Definition of angles α, ϕ, φ . Right: Photon momentum \vec{k} and polarization $\vec{\epsilon}$ define the beam polarization plane while the reaction plane is defined by the recoil proton p and produced meson M	33

List of Tables

1.1	Summary of the particles of the SM	1
1.2	Allowed quantum numbers for the intermediate resonance state N^*/Δ^*	4
3.1	The five most probable decay modes of the η' meson. The most probable further decay with according branching ratio is shown in brackets.[pdg]	11
3.2	Examined MC reactions that were used in sum for the fit	16
3.3	Fit functions and cut ranges for each variable	17
3.4	Total cross sections σ in the energy range 1 500 to 1 800 MeV, branching ratios (BR) to $n\gamma$ final states and maximum acceptance \tilde{A} for signal and possible background contributions	23
3.5	Relative loss in signal and background events if a cut on ΔE is applied.	29